



Electrospun β -Mo₂C/CNFs as an efficient sulfur host for rechargeable lithium sulfur battery

Ruiyuan Zhuang¹ · Shanshan Yao¹ · Xiangqian Shen^{1,2} · Tianbao Li² · Shibiao Qin² · Jianhong Yang³

Received: 8 September 2018 / Accepted: 16 January 2019 / Published online: 23 January 2019
© Springer Science+Business Media, LLC, part of Springer Nature 2019

Abstract

Lithium–sulfur (Li–S) battery with a high energy density is being considered the promising energy storage devices. However, it is a challenge to develop high performance electrodes for commercialization of rechargeable Li–S battery system because of the dissolution of polysulfides during charging and discharging process and the insulating nature of sulfur. In this work, we firstly demonstrate the novel host material of β -molybdenum carbide/carbon nanofibers (β -Mo₂C/CNFs) with good electrical conductivity and porous structure, which is synthesized via the facile one-pot electrospinning method and subsequent thermal treatment to impregnate sulfur in Li–S battery. The as-prepared β -Mo₂C/CNFs act as polysulfide reservoirs to alleviate the shuttle effect by the physical and chemical adsorption. Meanwhile, the mesoporous structure of β -Mo₂C/CNFs can facilitate the electron transport for surface reactions and improve the reaction kinetics. It is demonstrated that β -Mo₂C/CNFs/sulfur composite displays a high lithium-ion diffusion coefficient, a low interfacial resistance and excellent electrochemical performance than that of CNFs/sulfur and pure sulfur.

1 Introduction

Lithium-sulfur (Li–S) battery with the theoretical capacity of 2600 Wh kg⁻¹ offers considerable promise for energy storage applications. However, it has a few drawbacks, such as insulating of sulfur and the shuttle effect caused by the dissolved polysulfides in electrolyte. To address these problems, there have been substantial researches conducted with focus on sulfur cathode structures with the approaches of dispersing or trapping sulfur into host which

is both conductive and the capability of adsorbing sulfur or lithium polysulfides. A variety different conductive carbon and conductive polymers have been applying as additives to enhance electrochemical performance of Li–S battery [1–3]. Additionally, several oxides including SiO₂, Al₂O₃ and MnO₂ were found to be highly effective for polysulfides entrapment. However, these oxides usually have intrinsically poor electrical conductivity, thus the chemical adsorbed polysulfides are difficult to be reduced directly on the hosts surface, resulting in relatively lower sulfur utilization [4–6]. Recently, the conductive of metal oxide/sulfides, such as Ti₄O₇ nanoparticles [7, 8] and Co₉S₈ [9] nanosheets have been employed as sulfur hosts with both good conductivity and polar nature. Goodenough and co-workers reported that electrically conductive titanium nitride (TiN) as the host can efficiency confines the polysulfides [10]. The TiN based sulfur cathodes show much better electrochemical performance as compared with TiO₂/sulfur, which ascribed to electrical conductivity of TiN. Meanwhile, nitrides and carbides such as Mo₂N, VN, Ti₂C and Ti₃C₂ have been used for lithium-sulfur batteries [10–14]. Consequently, a novel conductive matrix is feasible direction for Li–S battery.

Molybdenum carbide, one of the most important compounds among transition metal carbides, due to its promising physical and chemical properties, such as high melting temperature, high resistance to corrosion and oxidation, catalytic

Electronic supplementary material The online version of this article (<https://doi.org/10.1007/s10854-019-00755-w>) contains supplementary material, which is available to authorized users.

✉ Shanshan Yao
yaosshan@ujs.edu.cn

¹ Institute for Advanced Materials, School of Materials Science and Engineering, Jiangsu University, Zhenjiang 212013, People's Republic of China

² Hunan Engineering Laboratory of Power Battery Cathode Materials, Changsha Research Institute of Mining and Metallurgy, Changsha 410012, People's Republic of China

³ Institute of Green Materials and Metallurgy, School of Materials Science and Engineering, Jiangsu University, Zhenjiang 212013, People's Republic of China

properties and good electrical conductivity (102 S cm^{-1}) [15]. We herein for the first time report a facile route based on a single-spinneret electrospinning with subsequent annealing process, for the fabrication of $\beta\text{-Mo}_2\text{C}$ /carbon nanofibers ($\beta\text{-Mo}_2\text{C}/\text{CNFs}$) as the host to encapsulate sulfur. For application as the cathode material of lithium-sulfur battery, the $\beta\text{-Mo}_2\text{C}/\text{CNFs}/\text{S}$ cathode exhibits better electrochemical performance than the pristine sulfur cathode.

2 Experimental

2.1 Synthesis and characterization of $\beta\text{-Mo}_2\text{C}/\text{CNFs}$ /sulfur

Typically, a 10 wt% polyacrylonitrile (PAN, $M_w = 150,000$) solution was first prepared by dissolving PAN powder in *N,N*-dimethylformamide under stirring at room temperature for 12 h. In the preparation of PAN/phosphomolybdic (PMA $\text{H}_3\text{PO}_4 \cdot 12\text{MO}_3$) solution, 3 g of PMA was dissolved in as-prepared PAN solution to form a homogeneous viscous solution, which was loaded into a plastic syringe pump with a capillary. A high voltage power supply was used to provide a voltage of 15 kV to the needle tip and the rotating drum collector covered by aluminum foil, serving as the counter electrode. To ensure a stable electrospinning, the solution was fed at a rate of 0.5 mL h^{-1} , the distance between the needle tips and drum collectors was fixed at 18 cm. Finally, the as-electrospun nanofibers were pre-oxidized at $260 \text{ }^\circ\text{C}$ for 2 h in air and calcined at $950 \text{ }^\circ\text{C}$ for 4 h in argon to obtain $\beta\text{-Mo}_2\text{C}/\text{CNFs}$. CNFs were prepared without adding PMA in the precursor solution, followed with the same pyrolysis as above.

$\beta\text{-Mo}_2\text{C}/\text{CNFs}/\text{sulfur}$ ($\beta\text{-Mo}_2\text{C}/\text{CNFs}/\text{S}$) composites were synthesized by a typical approach of melt-diffusion method. The mixture was well mixed by $\beta\text{-Mo}_2\text{C}/\text{CNFs}$ and sublimed sulfur with a weight ratio of 1:1, then was heated at $155 \text{ }^\circ\text{C}$ for 6 h in a sealed teflon-lined stainless-steel autoclave. After cooling to room temperature, the $\beta\text{-Mo}_2\text{C}/\text{CNFs}/\text{S}$ composites were obtained.

2.2 Materials characterization

The product was measured by X-ray diffraction (XRD, Rigaku D/Mmax 2500 PC) and laser-Raman spectroscopy (Raman, Thermo Fisher). The Brunauer-Emmett-Teller (BET) surface area was determined by nitrogen adsorption-desorption using a NOVA 3000 e analyzer. The morphology of the fibers was determined by scanning electron microscopy (SEM, JSM-7001F). Detailed structural and morphological characterization were performed by using high-resolution transmission electron microscopy (Tecnai G2 F30), operated at 200 kV accelerating voltage. Selected

specimens were examined with energy-dispersive X-ray (EDX) spectroscopy and elemental mapping facilities, which were attached to the HRTEM. X-ray photoelectron spectroscopy (XPS, Thermo Scientific ESCALALB 250Xi) was also adopted to analyze the surface compositions. The contents of $\beta\text{-Mo}_2\text{C}$ in the $\beta\text{-Mo}_2\text{C}/\text{CNFs}$ hybrids were measured using thermogravimetric (TG, Q 600) analysis in the temperature range of $25\text{--}700 \text{ }^\circ\text{C}$ under an air flow with a heating rate of 10 K min^{-1} . The sulfur content of $\beta\text{-Mo}_2\text{C}/\text{CNFs}/\text{S}$ composites was characterized by elemental analysis (elementer analyses system GmbH).

To characterize the properties of $\beta\text{-Mo}_2\text{C}/\text{CNFs}/\text{S}$ from cycled electrodes, the Li-S coin cell after designated cyclic tests were transferred into the glove box and disassembled. The cycled interlayer was repeatedly rinsed with tetrahydrofuran (THF) and vacuum dried at $50 \text{ }^\circ\text{C}$ for 12 h to remove the residual solvent for further measurements.

Moreover, for the visualized adsorption characterization, a Li_2S_6 solution was synthesized by adding Li_2S and sulfur with a molar ratio of 1:5 in THF under stirring according to literature [16]. The obtained solution of Li_2S_6 was used for the sulfide adsorption test. $\beta\text{-Mo}_2\text{C}/\text{CNFs}$ and nanosized conductive carbon (acetylene black: AB) were added into 10.0 mL of $\text{Li}_2\text{S}_6/\text{THF}$ solutions, respectively. The mixture was adequately stirred for 0.5 h for adsorption test. UV-visible absorption spectroscopy analysis (UV-1800PC, Shanghai Mapada Instrument Co. Ltd.) was carried out to evaluate the polysulfide adsorption capability of $\beta\text{-Mo}_2\text{C}/\text{CNFs}$ and AB.

2.3 Electrode fabrication and electrochemical measurement

The working electrode was fabricated by mixing the active material ($\text{Mo}_2\text{C}/\text{CNFs}/\text{S}$ or AB/S) with conducting additive (Super P Li) and a polyvinylidene fluoride in *N*-methyl-2-pyrrolidone with a weight ratio of 7:2:1. The active amount of sulfur loading is 1.5 mg cm^{-2} in the working electrode. The electrolyte was 1.0 M lithium bis(trifluoromethanesulfone)imide (LITFSI) in 1,3-dioxolane (DOL) and 1,2-dimethoxyethane (DME) (volume ratio 1:1) with 0.1 M LiNO_3 additive. About 75 μL electrolyte was added for each coin cells. CR2032-type coin cells were produced to evaluate the electrochemical performance of $\beta\text{-Mo}_2\text{C}/\text{CNFs}/\text{S}$. A lithium foil was used as the counter electrode as a polypropylene microsporous sheet (Celgard 2400) as the separator. The galvanostatic cycling of cells were performed in the voltage rang 1.7–2.8 V on LAND battery testing system ($1\text{C} = 1675 \text{ mA g}^{-1}$). Cyclic voltammetry (CV) measurements at a scan rate of 0.1 mV s^{-1} and electrochemical impedance spectra (EIS) tests in the frequency range of 100 kHz–100 mHz were using an electrochemistry workstation (VMP2).

3 Results and discussion

The XRD patterns of $\text{Mo}_2\text{C}/\text{CNFs}$, sublimated sulfur and $\text{Mo}_2\text{C}/\text{CNFs}/\text{sulfur}$ composite are presented in Fig. 1a. The diffraction peaks at 2θ of 34.5° , 38.1° , 39.5° , 52.2° , 61.6° , 69.6° , 74.7° and 75.6° , which are assigned to the planes of (1 0 0), (0 0 2), (1 0 1), (1 0 2), (1 1 0), (1 0 3), (1 1 2) and (2 0 1) of the hexagonal close-packed $\beta\text{-Mo}_2\text{C}$ crystalline phase [17]. The refinement gives the cell constants ($a = 3.0113 \text{ \AA}$, $c = 4.7383 \text{ \AA}$), which is consistent with the value reported in the literature ($a = 3.0124 \text{ \AA}$, $c = 4.7352 \text{ \AA}$) (JCPDS: 35-0787). And sulfur corresponding to an Fdd orthorhombic structure (JCPDS: 08-0247), respectively. As for $\beta\text{-Mo}_2\text{C}/\text{CNFs}/\text{S}$ composite, there are no any new phases in the final product except pure sulfur and $\beta\text{-Mo}_2\text{C}/\text{CNFs}$, which indicates that no chemical reaction between sulfur and $\beta\text{-Mo}_2\text{C}/\text{CNFs}$ occurred during the synthesis process. The Raman spectra of $\beta\text{-Mo}_2\text{C}/\text{CNFs}$ excited with 532 nm laser line is shown in Fig. 1b. It

consists of two characteristic bands, mainly those of the G (graphite) and D (defect) bands at ~ 1582 and $\sim 1349 \text{ cm}^{-1}$. The ratio of intensity of G/D bands is measure of an appreciable formation of graphitic carbon. Based on the XRD results, the $\beta\text{-Mo}_2\text{C}/\text{CNFs}$ were prepared via electrospinning with subsequent thermal treatment.

The textural properties of $\beta\text{-Mo}_2\text{C}/\text{CNFs}$ were obtained using N_2 adsorption–desorption measurements, as shown in Fig. 1c. The isotherms exhibit very similar type IV behavior at high relative pressure, with hysteresis loops, which are characteristic of mesoporous structures. In our case, the specific surface area of $\beta\text{-Mo}_2\text{C}/\text{CNFs}$ is $213.73 \text{ m}^2 \text{ g}^{-1}$. Calculation of the pore size distribution from desorption branch of the isotherm reveals a slightly bimodal pore size distribution with an average pore diameter according to Barrett–Joyner–Halenda (BJH) of 6.7 nm (Fig. 1d).

The content of $\beta\text{-Mo}_2\text{C}$ in the $\beta\text{-Mo}_2\text{C}/\text{CNFs}$ hybrids were measured by TG (Fig. S1a). It can be seen that the residues after oxidation in air is 73.7% for the $\beta\text{-Mo}_2\text{C}/\text{CNFs}$. The final product after the whole TG analysis was confirmed

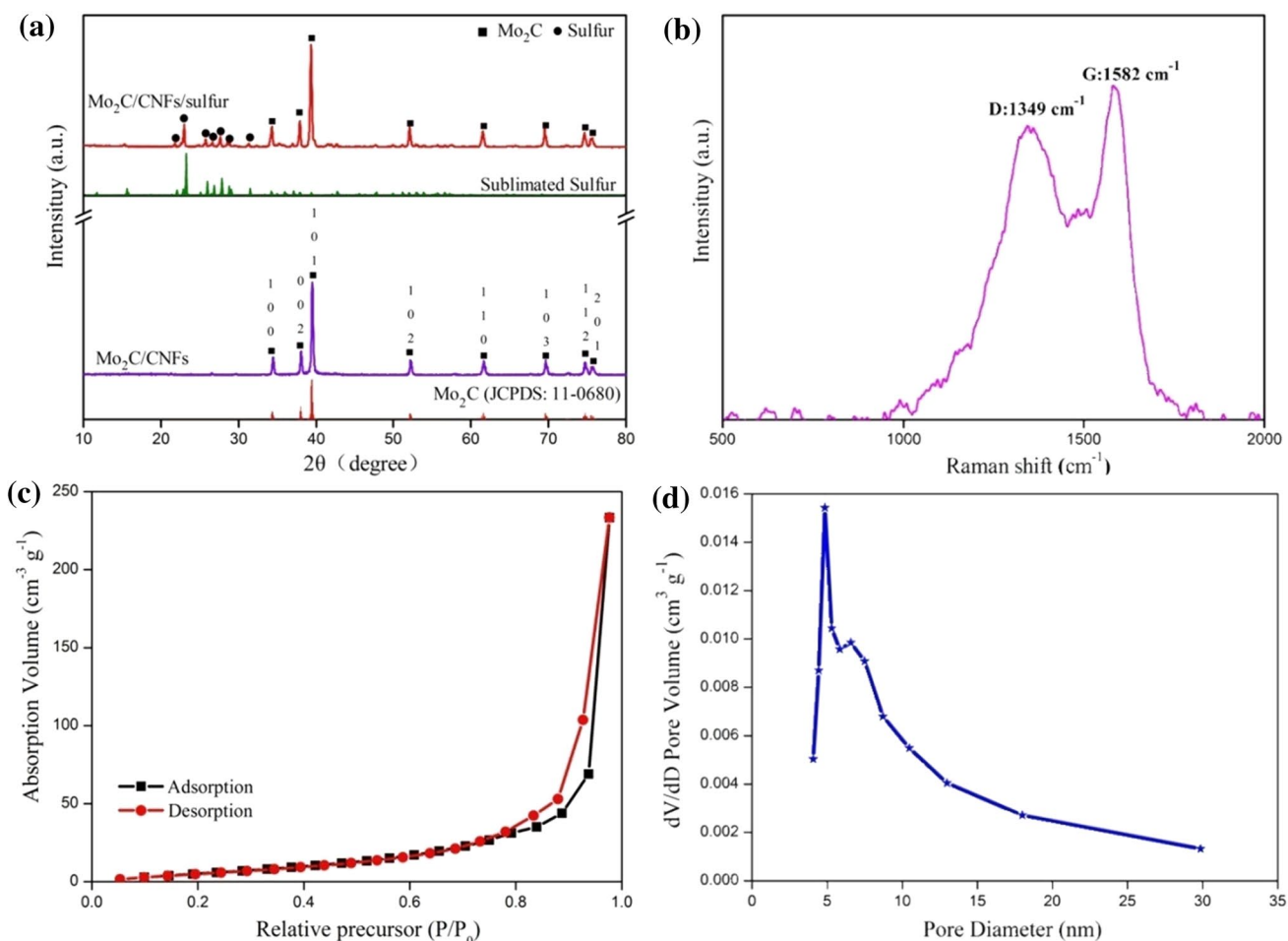


Fig. 1 a XRD patterns of $\beta\text{-Mo}_2\text{C}/\text{CNFs}$, sublimated sulfur and $\beta\text{-Mo}_2\text{C}/\text{CNFs}/\text{sulfur}$ composite; b Raman spectra of $\beta\text{-Mo}_2\text{C}/\text{CNFs}$; c N_2 adsorption–desorption isotherms and d BJH pore size distribution of $\beta\text{-Mo}_2\text{C}/\text{CNFs}$

to be MoO_3 (JCPDS: 05-0508) according to Fig. S1b. As a result, the $\beta\text{-Mo}_2\text{C}$ loadings in the $\beta\text{-Mo}_2\text{C}/\text{CNFs}$ were calculated to be 25.5%. Meanwhile, elemental analysis confirmed the presence of sulfur in the $\beta\text{-Mo}_2\text{C}/\text{CNFs}/\text{S}$ and the average sulfur content in the $\beta\text{-Mo}_2\text{C}/\text{CNFs}/\text{S}$ was 48.2%.

The SEM and TEM images of $\beta\text{-Mo}_2\text{C}/\text{CNFs}$ are shown in Fig. 2a, b, respectively. As can be seen from Fig. 2a, the as-synthesized $\beta\text{-Mo}_2\text{C}/\text{CNFs}$ have the diameter of about 700 nm and the length of several microns. This kind of fibrous porous structure has the advantages of facilitating electron transport and adsorbing polysulfides during the charging/discharging process. To further understand the porous structure of $\beta\text{-Mo}_2\text{C}/\text{CNFs}$ sample, TEM measurements were studied. Figure 2b indicates that the sample has a porous fibers-like aggregation of nanosized crystallites. EDX spectrum confirmed the existence of elements Mo

and C (Fig. 2c). Here, the peaks of Cu come from copper net. HRTEM image showed in Fig. 2d indicates that the grown structure is single crystalline with lattice spacing of 0.228 nm which corresponds to the [1 0 1] crystal planes of the hexagonal close-packed $\beta\text{-Mo}_2\text{C}$. Elemental mapping images (Fig. 2e) of $\beta\text{-Mo}_2\text{C}/\text{CNFs}$ indicate that Mo and C are homogeneously distributed throughout the composite. Figure 2f, g show the SEM images of sulfur cathode without $\beta\text{-Mo}_2\text{C}/\text{CNFs}$ doping and with $\beta\text{-Mo}_2\text{C}/\text{CNFs}$ doping. The SEM is shown that after the addition of the $\beta\text{-Mo}_2\text{C}/\text{CNFs}$, the sulfur morphology was drastically changed from smooth to rough agglomerated particles. To further determine the distribution of $\beta\text{-Mo}_2\text{C}/\text{CNFs}$ in the $\beta\text{-Mo}_2\text{C}/\text{CNFs}/\text{S}$ composite, the EDS mapping of the composite are shown in Fig. 2h. The $\beta\text{-Mo}_2\text{C}/\text{CNFs}$ could be homogeneously dispersed into the sulfur. Moreover, the smaller particle size

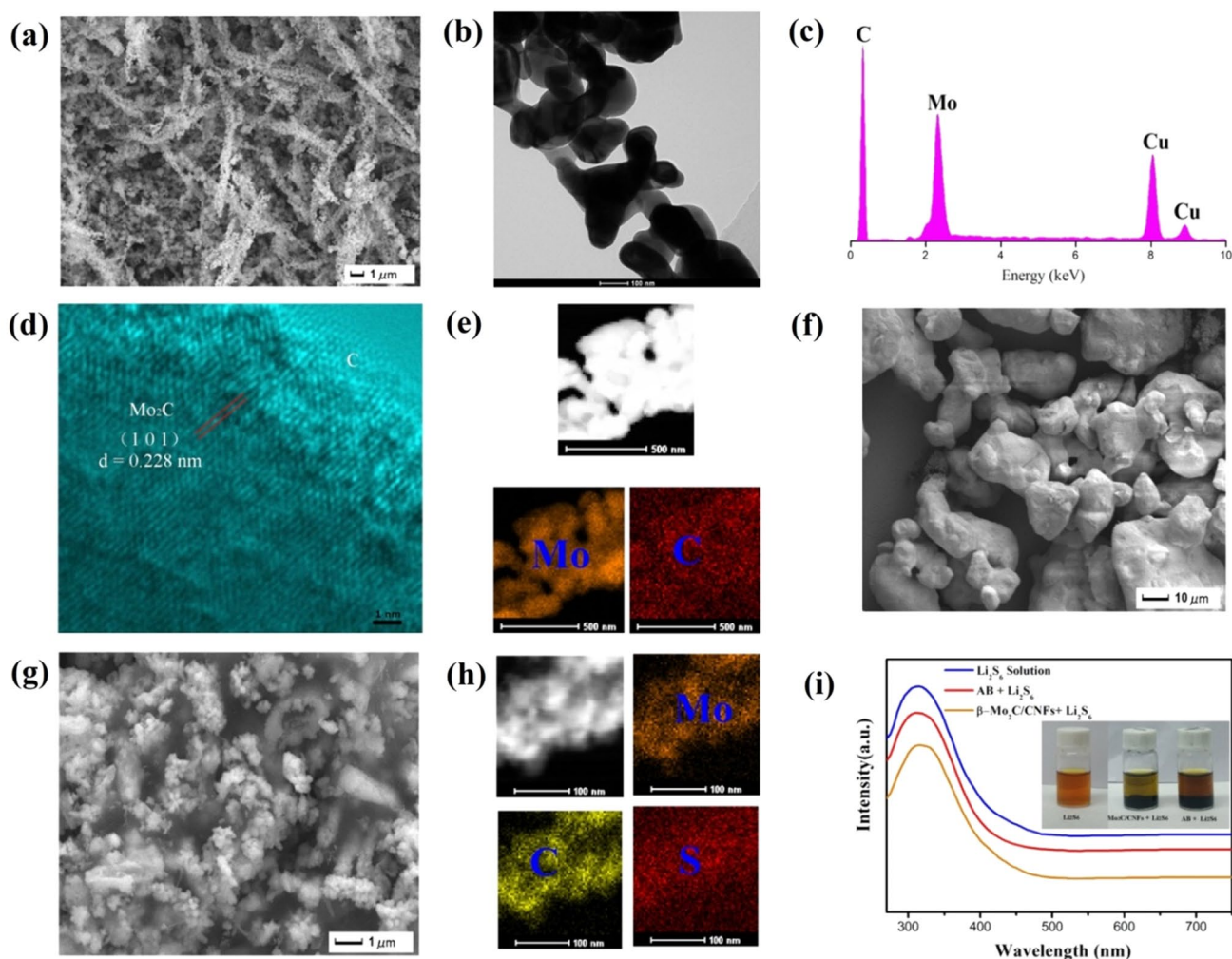


Fig. 2 a, b SEM and TEM images of $\beta\text{-Mo}_2\text{C}/\text{CNFs}$; c, d EDX line analysis and HRTEM image of $\beta\text{-Mo}_2\text{C}/\text{CNFs}$; e EDX elemental mapping images of the $\beta\text{-Mo}_2\text{C}/\text{CNFs}$; f, g SEM images of sublimated sulfur and $\beta\text{-Mo}_2\text{C}/\text{CNFs}/\text{sulfur}$ composite; h EDX elemental

mapping images of the $\beta\text{-Mo}_2\text{C}/\text{CNFs}/\text{sulfur}$; i UV-vis absorption spectra of Li_2S_6 solution before and after the addition of $\beta\text{-Mo}_2\text{C}/\text{CNFs}$ and AB. Inset is the photograph of sealed vials of a $\text{Li}_2\text{S}_6/\text{THF}$ solution after contact with $\beta\text{-Mo}_2\text{C}/\text{CNFs}$ and AB after 0.5 h

could favor the ion diffusivity in the cathode due to the reduction in the lithium ions pathways. In order to compare the polysulfide adsorption capability of $\beta\text{-Mo}_2\text{C/CNFs}$ and AB, UV–visible absorption spectroscopy was used to analyze the concentration variation of Li_2S_6 solution. As demonstrated in Fig. 2i, the polysulfide solution peak located at approximately 300 nm can be ascribed to S_6^{2-} species [18]. After absorption for 0.5 h, a large decrease in the absorption peak intensity of the solution with $\beta\text{-Mo}_2\text{C/CNFs}$ at 300 nm was identified and confirmed the improved absorption capability of the $\beta\text{-Mo}_2\text{C/CNFs}$ composite fibers for polysulfides.

The XPS results were also used to identify the surface energy change of $\beta\text{-Mo}_2\text{C/CNFs}$. The binding energies of all the elements are calibrated using $\text{C1s} = 284.6$ eV as a references. As shown in Fig. 3a, the survey spectrum of the pristine $\beta\text{-Mo}_2\text{C/CNFs}$ shows distinct signals at 231.8, 285.2, 396.8, 414.3, and 531.4 eV, which can be assigned to Mo 3d, C1s, Mo3p_{3/2}, Mo3p_{1/2} and O1s, respectively. Figure 3b shows the high resolution XPS spectrum of Mo3d, which shows two major peaks with binding energies of 227.3 and 232.0 eV, and two weak peaks at 229.4 and 234.8 eV [19]. The former two peaks can be ascribed to Mo3d of $\beta\text{-Mo}_2\text{C}$ and the latter two peaks to oxidized molybdenum with intermediate oxidation states (MoO_x). The MoO_x may result from the slight surface oxidation of metastable of $\beta\text{-Mo}_2\text{C}$ in air.

The cell after 50 cycles discharge is disassembled in the glovebox, and the $\beta\text{-Mo}_2\text{C/CNFs/S}$ composite repeatedly rinsed with THF are dried for XPS characterization. Figure 3c confirms the elemental composition of after cycled $\beta\text{-Mo}_2\text{C/CNFs}$ with peaks of Mo, C, S and O present. The S_{2p} spectrum is deconvoluted into three different signals with binding energies of 164.3, 169.6 and 171.2 eV attributed to the overlapped S–S band from the sulfur, SO_3^{2-} from the decomposition of electrolyte, and sulfate (S–O) by the oxidation of sulfur, respectively (Fig. 3d) [20–22]. After cycled discharge, the deconvoluted Mo 3d XPS spectra of $\beta\text{-Mo}_2\text{C/CNFs/S}$ are similar to pristine $\beta\text{-Mo}_2\text{C/CNFs}$ expect that the binding energies of Mo 3d_{5/2} and Mo 3d_{3/2} for Mo^{2+} slightly shift to the higher values of 227.6 and 232.3 eV, respectively (Fig. 3e). The reason should also be related to the presence of SO_3^{2-} or S–O compounds on $\beta\text{-Mo}_2\text{C}$ surface, the electron-withdrawing ability of which could increase the valence state of Mo^{6+} . Furthermore, the reduction of Mo^{6+} is observed in our work, which is probably a reduction of Mo valence state from Mo^{6+} to Mo^{4+} due to the formation of SO_3^{2-} on MoO_x surface. In addition, the good electronic conductance of $\beta\text{-Mo}_2\text{C/CNFs}$ could also facilitate the transport of electrons from $\beta\text{-Mo}_2\text{C}$ surface to SO_3^{2-} and S–O species. All these results suggest a strong S–O binding interaction between sulfur and Mo_2C matrix,

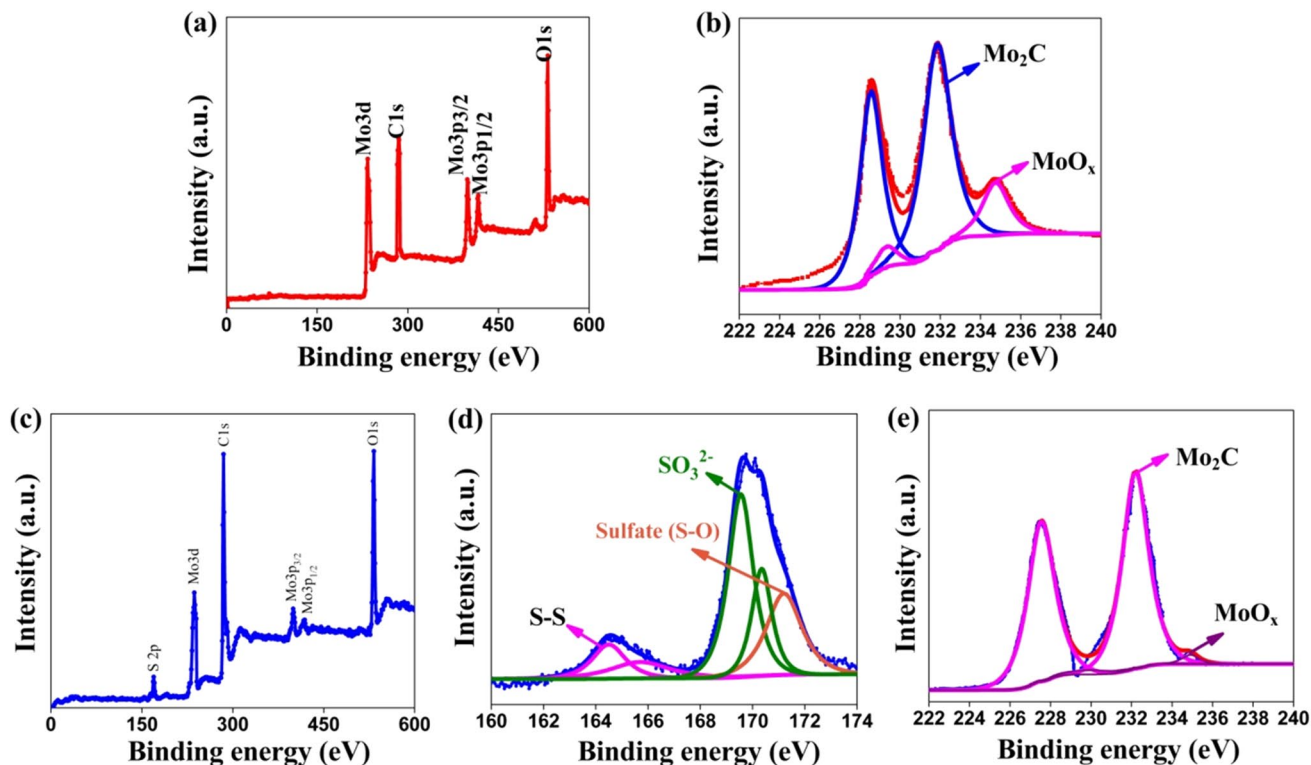


Fig. 3 XPS spectra of pristine $\beta\text{-Mo}_2\text{C/CNFs}$: **a** survey spectrum and **b** high-resolution of Mo 3d spectra; and after cycled $\beta\text{-Mo}_2\text{C/CNFs}$: **c** survey spectrum and high-resolution of **d** S_{2p} and **e** Mo3d spectra

which is expected to play the function of anchoring sulfur and preventing the subsequently formed polysulfides from dissolving into electrolyte during charge–discharge process.

Electrochemical measurements of the assemble coin cells were then performed in a voltage cutoff window of 1.7–2.8 V. Figure 4a show the voltammogram profiles. Two typical characteristic peaks are located at 2.20 and 2.00 V, corresponding to the electrochemical processes of active sulfur to long-chain polysulfides (Li_2S_x , $4 \leq x \leq 8$) and conversion of insoluble $\text{Li}_2\text{S}/\text{Li}_2\text{S}_2$ from dissolved polysulfides, respectively [23, 24]. The oxidation peak around 2.40 V is corresponds to the transformation of Li_2S_2 and Li_2S into the Li_2S_8 . No additional peaks were associated with $\beta\text{-Mo}_2\text{C}/\text{CNFs}$, confirming that the additives are not electrochemically active in the selected voltage region. Here, compared with pure sulfur cathode, $\beta\text{-Mo}_2\text{C}/\text{CNFs}/\text{S}$ composite cathode exhibits the smaller electrochemical polarization (lower voltage hysteresis, ΔV), suggesting a highly facile electrochemical redox reaction and low resistance [25, 26].

Furthermore, an interesting point to note is that the highest current densities of the $\beta\text{-Mo}_2\text{C}/\text{CNFs}/\text{S}$, indicating enhanced reaction kinetics in charge–discharge process.

Figure 4b presents the cycling performance of the cells assembled from sulfur cathodes with and without $\beta\text{-Mo}_2\text{C}/\text{CNFs}$. The cell assembled with pure sulfur electrode revealed lower initial discharge capacities. After a few cycles, the discharge capacity reduced from 587 to 220 mAh g^{-1} . The $\beta\text{-Mo}_2\text{C}/\text{CNFs}/\text{S}$ composite cathode can deliver an initial discharge capacity of 1017 mAh g^{-1} and reversible capacity remains at 767 mAh g^{-1} after 50 cycles. The improved cycling performance with presence of $\beta\text{-Mo}_2\text{C}/\text{CNFs}$ could be attributed to the polysulfides adsorption and improved electrochemical reaction kinetics of $\beta\text{-Mo}_2\text{C}$, demonstrated by the initial specific capacity and CV curves. Meanwhile, the electrochemical performance of $\beta\text{-Mo}_2\text{C}/\text{CNFs}$ matrix for application in Li–S batteries is also compared with several other carbon nanofibers and metal oxides fibers (Table 1), with further

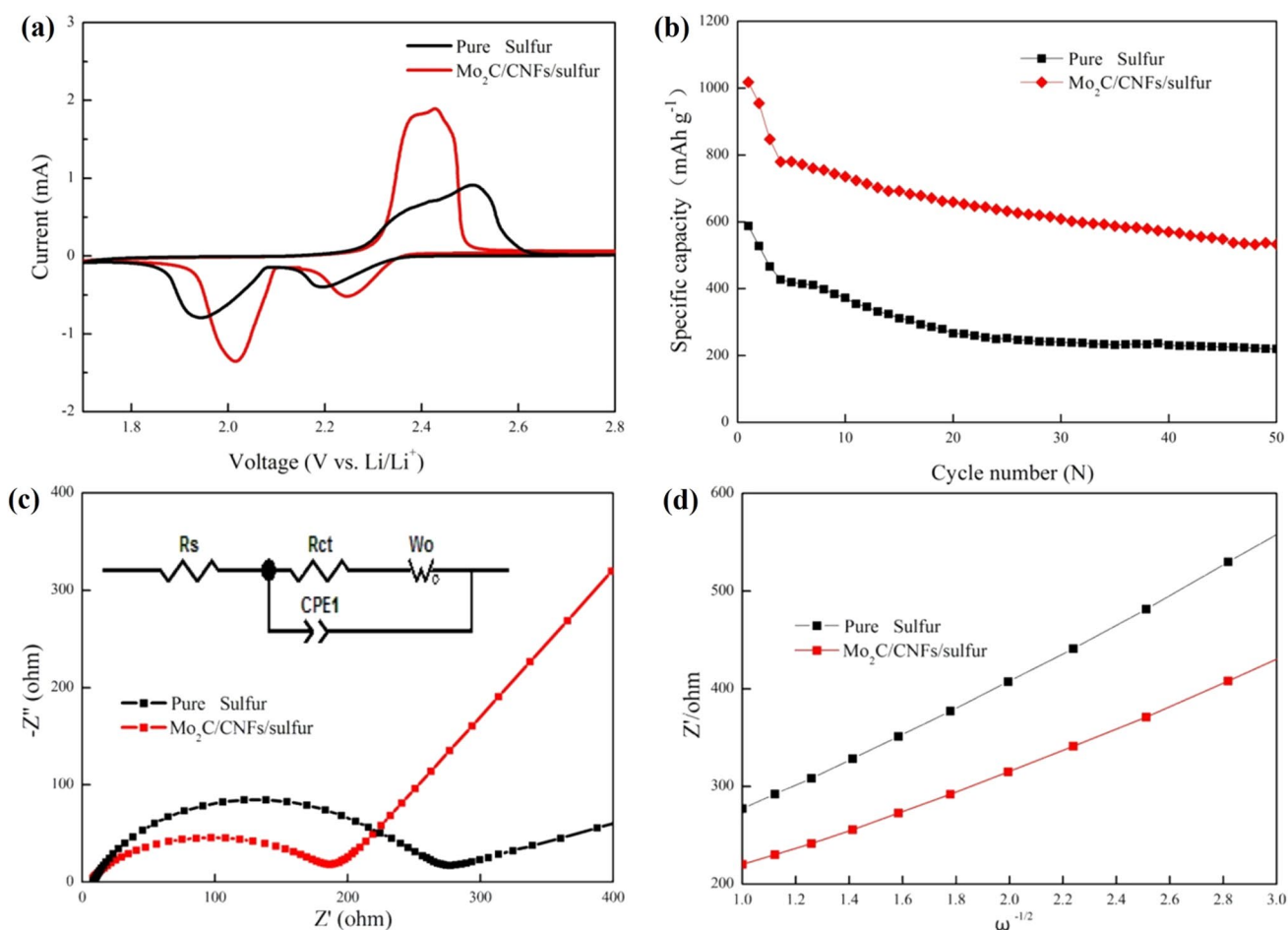


Fig. 4 Electrochemical performance of $\beta\text{-Mo}_2\text{C}/\text{CNFs}/\text{sulfur}$ and pure sulfur electrode: **a** CV with a sweep rate of 0.1 mV s^{-1} ; **b** The cycle performance at 0.25 mA cm^{-2} ; **c** EIS spectra and **d** the depend-

ence of Z''_{re} on the reciprocal square root of the frequency $\omega^{-1/2}$ in the low-frequency region for the sublimated sulfur and $\beta\text{-Mo}_2\text{C}/\text{CNFs}/\text{sulfur}$ composite electrodes

Table 1 The electrochemical performance comparison of β -Mo₂C/CNFs with other matrices for application in Li–S batteries

Matrix	Cycle performances
Carbon nanofibers (CNFs) [27]	207 mAh g ⁻¹ 0.1C per 50 cycles
CNFs [28]	390 mAh g ⁻¹ 0.1C per 100 cycles
Vapor grown carbon fibers (VGCFs) [29]	335 mAh g ⁻¹ 0.1C per 40 cycles
CNFs [30]	560 mAh g ⁻¹ 0.1C per 50 cycles
Mg _{0.6} Ni _{0.4} O fibers [31]	435 mAh g ⁻¹ 0.1C per 20 cycles
β -Mo ₂ C/CNFs [This work]	767 mAh g ⁻¹ 0.25 mA cm ⁻² (\approx 0.1C) per 50 cycles

Table 2 Electrochemical impedance parameters of the samples

Electrodes	R _s (Ω)	R _{ct} (Ω)	D _{Li} (cm ² s ⁻¹)
β -Mo ₂ C/CNFs/S	1.33	168.39	8.42 \times 10 ⁻¹⁴
Pure sulfur	2.07	277.35	4.38 \times 10 ⁻¹⁴

demonstrates the electrochemical behaviors of β -Mo₂C/CNFs/S composite cathode.

The potential mechanism for such different electrochemical performance is further excavated by the EIS test. In order to further understand the β -Mo₂C/CNFs in the role of electrochemical reaction, the relevant equivalent circuit mode is presented. In the spectrum, the number of semi-circle depends on the depth of the discharge and charge. The Nyquist plot consists of a semicircle at high to medium frequency region and sloping line at low frequency region, which are referred to the charge-transfer reaction and lithium ions diffusion in the solid electrode material [32]. The EIS is simulated using the equivalent circuit as shown in the inset of Fig. 4c, in which R_s is the resistance of electrolyte, R_{ct} reflects the charge-transfer resistance, CPE representative double-layer capacitance considering the surface roughness of particles [33]. The slope line corresponds to the Warburg impedance, represented by W_l. The fitting results are listed in Table 2. As shown in Fig. 3c, the charge transfer of β -Mo₂C/CNFs/S composite cathode (R_{ct} = 168.39 Ω) is smaller than of sulfur cathode (R_{ct} = 277.35 Ω). The result suggests that the sample has a better lithium ions transfer than pure sulfur electrode. To further confirm this result, the lithium ion diffusion coefficient is calculated by the following Eq. (1) [34]:

$$D_{Li^+} = \frac{R^2 T^2}{2A^2 n^4 F^4 C^2 \sigma^2} \quad (1)$$

where D_{Li⁺} represents the diffusion coefficient of the lithium ion, R is the gas constant, T is the absolute temperature, A is the surface area of electrode, n is the number of electron per molecule during reaction, F is the Faraday constant, C is the concentration of lithium ion, and σ is the Warburg factor which can be calculated from Eq. (2) [35]:

$$Z_{re} = R_e + R_{ct} + \sigma \omega^{-1/2} \quad (2)$$

σ are the slope for the plots of Z_r versus the reciprocal root square of the lower angular frequencies ($\omega^{-1/2}$), which is presented in Fig. 4d. Similarly, the σ of the β -Mo₂C/CNFs/S is far lower than that of pure sulfur electrode, demonstrating the faster diffusion. This can be explained that by the effective immobilization of the β -Mo₂C/CNFs for the dissolvable long-chain polysulfides, which prevents the formation of solid electrolyte interface on the anode arising from the deposition of the shorter-chain lithium polysulfides [36]. Therefore, the excellent performance of the ternary β -Mo₂C/CNFs/S composites can be attributed to three major factors: (1) the well-developed mesoporous structure contributes to trap dissolved lithium polysulfides in the positive electrode; (2) the strong chemisorption ability of β -Mo₂C/CNFs; (3) the electrical conductivity of β -Mo₂C/CNFs effectively localizes the soluble polysulfides species with cathode and facilitates electron and lithium ions transport to/from the cathode materials. These positive factors contribute to a slight modification of the cathode with β -Mo₂C/CNFs profoundly improved the electrochemical performance of Li–S battery.

4 Conclusion

In summary, we have crafted a mesoporous structure of β -Mo₂C/CNFs by electrospinning technology. The obtained β -Mo₂C/CNFs have been applied to the sulfur host for Li–S battery and shown to exhibit high capacities when compared to electrodes with pure sulfur. The improved electrochemical performance could be attributed to the adsorption of polysulfides and acceleration of the electrochemical reaction kinetics during the charge–discharge process. The EIS results demonstrated that β -Mo₂C/CNFs/S composite displays a markedly higher lithium ions diffusion coefficient, a low interfacial resistance and much better electrochemical performance than the pristine sulfur cathode. The β -Mo₂C/CNFs provide an approach to improve the electrochemical properties of sulfur-based cathodes and has great potential in Li–S battery.

Acknowledgements This work was financially supported by the National Natural Science Foundation of China (Grant Nos. 51874146, 51504101), the China Postdoctoral Science Foundation (Grant Nos. 2018T110551, 2017M621640), the Six Talent Peaks Project of Jiangsu Province (XCL-125), the Natural Science Foundation of Jiangsu Province (Grant No. BK20150514), the Natural Science Foundation of Jiangsu Provincial Higher Education of China (Grant No. 15KJB430006), the Start-up Foundation of Jiangsu University for Senior Talents (Grant No. 15JDG014).

References

1. X. Yang, L. Zhang, F. Zhang, Y. Huang, Y.S. Chen, *ACS Nano* **8**, 5208–5215 (2011)
2. A. Manthiram, Y.Z. Fu, S.H. Chuang, C.X. Zu, Y.S. Su, *Chem. Rev.* **114**, 11751–11787 (2014)
3. Q. Pang, X. Liang, C.Y. Kwok, L.F. Nazar, *Nat. Energy* **1**, 16132 (2016)
4. X.L. Ji, S. Evers, R. Black, L.F. Nazar, *Nat. Commun.* **2**, 325 (2011)
5. M.Q. Liu, J.L. Hou, J. Xiang, X.Q. Shen, K.J. Luan, Y.J. Zhang, *J. Nanosci. Nanotechnol.* **18**, 7824–7829 (2018)
6. X. Liang, C. Hart, Q. Pang, A. Garsuch, T. Weiss, L.F. Nazar, *Nat. Commun.* **6**, 5682 (2015)
7. S.S. Yao, S.K. Xue, Y.J. Zhang, X.Q. Shen, X.Y. Qian, T.B. Li, K.S. Xiao, S.B. Qin, J. Xiang, *J. Mater. Sci* **28**, 7264–7270 (2017)
8. Y.J. Zhang, S.S. Yao, R.Y. Zhuang, K.J. Luan, X.Y. Qian, J. Xiang, X.Q. Shen, T.B. Li, K.S. Xiao, S.B. Qin, *J. Alloys Compd.* **729**, 1136–1144 (2017)
9. Q. Pang, D. Kundu, L.F. Nazar, *Mater. Horiz.* **3**, 130–136 (2016)
10. D.K. Nandi, U.K. Sen, D. Choudhury, S. Mitra, S.K. Sarkar, *ACS Appl. Mater. Interfaces* **6**, 6606–6615 (2014)
11. Z.H. Sun, J.Q. Zhang, L.C. Yin, G.J. Hu, R.P. Fang, H.-M. Cheng, F. Li, *Nat. Commun.* **8**, 14627 (2017)
12. X. Liang, A. Garsuch, L.F. Nazar, *Angew. Chem. Int. Ed.* **54**, 3907–3911 (2015)
13. X.Q. Zhao, M. Liu, Y. Chen, B. Hou, N. Zhang, B.B. Chen, N. Yang, K. Chen, J.L. Li, L. An, *J. Mater. Chem. A* **3**, 7870–7876 (2015)
14. C. Lin, W.K. Zhang, L. Wang, Z.Q. Wang, W. Zhao, W.H. Duan, Z.Q. Zhao, B. Liu, J. Jin, *J. Mater. Chem. A* **4**, 5993–5998 (2016)
15. Q.L. Sun, Y. Dai, Y.D. Ma, T. Jin, W. Wei, B.B. Huang, *J. Phys. Chem. Lett.* **7**, 937–943 (2016)
16. Q. Pang, D. Kundu, M. Cuisinier, L.F. Nazar, *Nat. Commun.* **5**, 4759 (2014)
17. W.F. Chen, C.H. Wang, K. Sasaki, N. Marinkovic, W. Xu, J.T. Muckerman, R.R. Adzic, *Energy Environ. Sci.* **6**, 943–951 (2013)
18. R.Y. Zhuang, S.S. Yao, M.X. Jing, X.Q. Shen, J. Xiang, T.B. Li, K.S. Xiao, S.B. Qin, *Beilstein J. Nanotechnol.* **9**, 262–270 (2018)
19. J.Y. Lei, Z.Q. Jiang, X.F. Lu, G.D. Nie, C. Wang, *Electrochim. Acta* **176**, 149–155 (2015)
20. Z. Yuan, H.J. Peng, J.Q. Huang, X.Y. Liu, D.W. Wang, X.B. Cheng, Q. Zhang, *Adv. Funct. Mater.* **24**, 6105–6112 (2014)
21. S.S. Yao, S.K. Xue, S.H. Peng, M.X. Jing, X.Y. Qian, X.Q. Shen, T.B. Li, Y.H. Wang, *J. Mater. Sci.* **20**, 17921–17930 (2018)
22. X.Y. Tao, J.G. Wang, Z.G. Ying, Q.X. Cai, G.Y. Zheng, Y.P. Gan, H. Huang, Y. Xia, C. Liang, W.K. Zhang, Y. Cui, *Nano Lett.* **14**, 5288–5294 (2014)
23. S. Yao, S. Xue, S. Peng, R. Guo, Z. Wu, X. Shen, T. Li, L. Wang, *Appl. Phys. A* **127**, 758 (2018)
24. H. Tang, S. Yao, M. Jing, X. Wu, J. Hou, X. Qian, D. Rao, X. Shen, X. Xi, K. Xiao, *Electrochim. Acta* **176**, 442–447 (2015)
25. Z.B. Xiao, Z. Yang, H.G. Nie, Y.Q. Lu, K.Q. Yang, S.M. Huang, *J. Mater. Chem. A* **2**, 8683–8689 (2014)
26. X. Wu, S. Yao, J. Hou, M. Jing, X. Qian, X. Shen, J. Xiang, X. Xi, *J. Nanosci. Nanotechnol.* **17**, 2482–2487 (2018)
27. S. Lu, Y. Cheng, X. Wu, J. Liu, *Nano Lett.* **13**, 2485–2489 (2013)
28. X.B. Yang, W. Zhu, G.B. Cao, X.D. Zhao, *RSC Adv.* **6**, 7159–7171 (2016)
29. Y.H. Wu, M.X. Gao, X. Li, Y.F. Liu, H.G. Pan, *J. Alloys Compd.* **608**, 220–228 (2014)
30. M.M. Rao, X.Y. Geng, X.P. Li, S.J. Hu, W.S. Li, *J. Power Sources* **212**, 179–185 (2012)
31. H. Tang, S.S. Yao, M.X. Jing, X. Wu, J.L. Hou, X.Y. Qian, D.W. Rao, X.Q. Shen, X.M. Xi, K.S. Xiao, *J. Alloys Compd.* **650**, 351–356 (2015)
32. X.B. Huang, X. Li, H.Y. Wang, Z.L. Pan, M.Z. Qu, Z.L. Yu, *Electrochim. Acta* **55**, 7362–7366 (2010)
33. N.A. Cañas, K. Hirose, B. Pascucci, N. Wagner, K.A. Friedrich, R. Hiesgen, *Electrochim. Acta* **97**, 42–51 (2013)
34. H. Tang, S. Yao, S. Xue, M. Liu, L. Chen, M. Jing, X. Shen, T. Li, K. Xiao, S. Qin, *Electrochim. Acta* **263**, 158–167 (2018)
35. A.Y. Shenouda, H.K. Liu, *J. Electrochem. Soc.* **157**, A1183–A1187 (2010)
36. C.Y. Fan, P. Xiao, H.H. Li, H.F. Wang, L.L. Zhang, H.Z. Sun, X.L. Wu, H.M. Xie, J.P. Zhang, *ACS Appl. Mater. Interfaces* **7**, 27959–27967 (2015)